JOURNAL OF SPACECRAFT AND ROCKETS
Vol. 35, No. 2, March–April 1998

Orbital and Configuration Influences on Spacecraft Dynamic Response

Stanley E. Woodard*
NASA Langley Research Center, Hampton, Virginia 23681-0001

Results of investigating the orbital and configuration influences on the Upper Atmosphere Research Satellite's dynamic response are presented. Orbital influences were due to temperature variation from crossing the Earth's terminator and variation of the solar incident energy as the orbit precessed. During the terminator crossing, the rapid ambient temperature change caused the spacecraft's two flexible appendages to experience thermal elastic bending (thermal snap). The resulting response was dependent on the orientation of the solar array and the solar incident energy. Orbital influences were also due to onboard disturbances, environmental disturbances, and spacecraft configuration changes resulting in dynamic responses that were repeated each orbit. Configuration influences were due to the solar array rotation's changing of the spacecraft modal properties. The orbital and configuration influences produced measurable spacecraft attitude variations as well as modal and amplitude trends in those variations.

Nomenclature

$\boldsymbol{A}$	= plant matrix
$\boldsymbol{B}$	= control influence matrix
$\boldsymbol{C}$	= output matrix
E	= beam modulus of elasticity
I	= beam area moment of inertia, ft-lb s^2
I_r, I_p, I_y	= space platform roll, pitch, and yaw inertia, respectively, ft-lb s^2
I_{tip}	= free-free beam rotational tip inertia, ft-lb s^2
$\mathcal{L}$	= beam length, ft
m_{tip}	= free-free beam tip mass, lb
t	= time, s
$\boldsymbol{U}$	= control torque input matrix
$\boldsymbol{X}$	= first-order state vector
$\boldsymbol{Y}$	= output vector
β	= complement of the angle between the orbit normal and the Earth-to-sun vector, deg
$\Gamma(\boldsymbol{X}, t)$	= mode shape matrix
$\theta(t)$	= vibration amplitude, deg
$\theta_{\max}$	= maximum vibration amplitude, deg
$\theta_{\min}$	= minimum vibration amplitude, deg
λ_n	= root of characteristic equation normalized by beam length, $\mathcal{L}$
$\lambda_n\mathcal{L}$	= root of characteristic equation for nth mode
ρ	= beam mass/unit length
ω_n	= natural frequency of nth mode, Hz
ω_0	= space platform orbital velocity, Hz

Introduction

FLIGHT data from the first 737 days after the launch of the Upper Atmosphere Research Satellite [UARS, launched Sept. 12, 1991 (Refs. 1–4)] were analyzed to determine the orbital and spacecraft configuration influences on spacecraft dynamic response. The spacecraft is shown in Fig. 1. Orbital influences were due to temperature variation from crossing the Earth's terminator and variation of the solar incident energy as the orbit precessed. Configuration influences were due to solar array rotation. The rotation changed spacecraft modal properties and the amount of solar energy incident upon the solar array. During the terminator crossing, the rapid ambient temperature change caused the spacecraft's two flexible appendages to experience thermal elastic bending (thermal snap). The resulting response was dependent on the orientation of the solar array and the solar incident energy. Orbital influences were also caused by onboard instrument and system motion, environmental disturbances from orbital temperature variation, and spacecraft configuration changes (due to solar array rotation), resulting in dynamic responses that were repeated each orbit.

The UARS' solar array rotated about an axis parallel to the spacecraft's pitch axis at a rotation rate that resulted in a complete revolution for each orbit. Solar array rotation kept the array facing the sun. The roll, pitch, and yaw axes are the X, Y, and Z axes, respectively, in Fig. 2. The solar array rotation was dynamically equivalent to the solar array being stationary and the spacecraft rotating about the solar array drive shaft. The UARS' yaw inertia was significantly higher than the roll inertia. During rotations, the inertia at the end of the drive shaft (tip inertia) would vary from the spacecraft roll inertia to the yaw inertia. The tip inertia, the modal properties of the solar array, and the response amplitude varied harmonically at twice the orbital frequency. Three effects were observed. The first was that, when the disturbances remained constant, the vibration amplitude varied inversely with the tip inertia.[3] A second effect was that variations of the tip inertia (boundary conditions) produced corresponding changes in the solar array frequencies of vibration and mode shapes.[3] The third effect that occurred because of the rotation of a flexible appendage was the variation of disturbance transmission resulting from the changing orientation of mode shapes.[3]

This paper presents the effects of orbital influences and configuration variation on spacecraft dynamic response. Previous papers published on UARS' in-flight dynamics in this journal have included Refs. 5 and 6. Reference 5 examined the analysis of payload–payload interaction and structure–payload interaction. The paper discussed the impact of UARS' solar array vibration and the disturbance due to the constant scanning motion of the High Resolution Doppler Imager (HRDI), which is mounted amidships on UARS, on the instrument pointing of the Halogen Occultation Experiment (HALOE, also mounted amidships on UARS). The disturbing frequencies of the solar array vibration and the HRDI scanning motion appeared as frequency modulations (similar to FM radio transmission) of the HALOE tracking frequency.[5] The analysis of the spacecraft's instrument and pointing interactions demonstrated that, on spacecraft with multiple scanning (or other disturbance-generating) instruments having stringent pointing tolerances, the disturbance of one instrument can confuse the pointing system of another. Reference 6 presented analysis of the UARS onboard instrument disturbance impact on the spacecraft attitude. Specifically, the impact of the solar array and high-gain antenna harmonic gear drive dynamics on the solar array vibration were discussed. Two solar array modes

Received Feb. 24, 1997; revision received Oct. 6, 1997; accepted for publication Oct. 14, 1997.

*Senior Research Engineer, Structural Dynamics Branch, Structures Division, MS 230. Member AIAA.

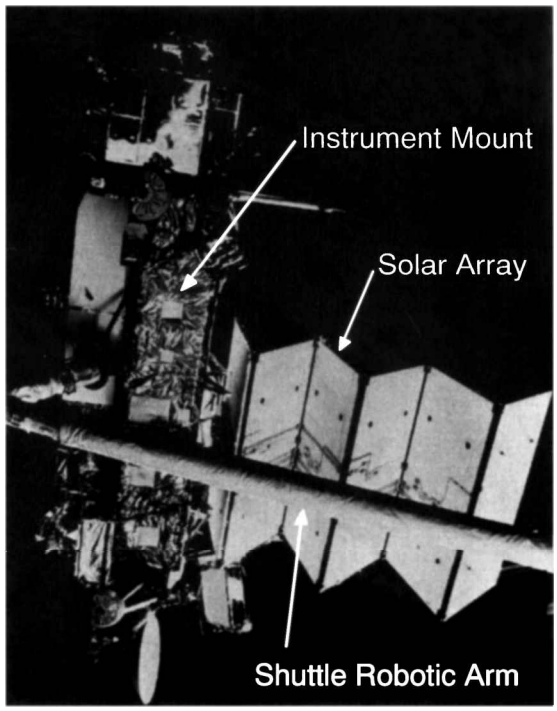

Fig. 1 UARS being released from the Space Shuttle Discovery's (STS-48) robotic arm.

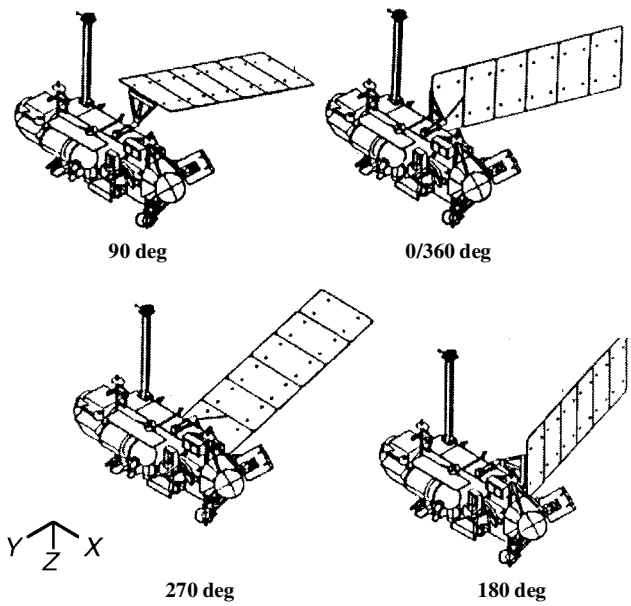

Fig. 2 UARS solar array positions.

of vibration were resonated by the output from both harmonic drives. The spacecraft attitude response was latitude specific. Furthermore, Ref. 6 identified and presented the impact of the high-gain antenna's static friction (stiction) on the spacecraft attitude.

After an overview of the UARS spacecraft, spacecraft jitter amplitude variation with tip inertia rotation is presented. Jitter is the angular excursion of an instrument's line of sight in a reference time interval (such as a sampling time period). The impact of solar array rotation direction and the solar incident energy on jitter amplitude is discussed afterward. Next, the spacecraft modal variation with tip inertia rotation is presented. The variation in inertia resulted in modal bands for the solar array's edgewise and flatwise modes. The flatwise and edgewise modes are transverse vibration about axes parallel to the roll and yaw axes, respectively. Three subsystem disturbances [the solar array harmonic drive, the high-gain antenna harmonic drive, and the Solar/Stellar Pointing Platform (SSPP) harmonic drive] had frequencies that overlapped the modal bands. The results of examining configuration and orbital variation on thermal bending of the solar array are presented next. The last section is an analysis of the disturbance transmission variation with appendage rotation.

UARS Overview

The UARS observatory (Fig. 1) included 10 science instruments, a high-gain antenna for communication links, the SSPP that carried three of the instruments, and an attitude control system. In addition to the suite of science instruments, UARS had a solar array consisting of six panels and an instrument extensional boom that were excited by disturbance sources onboard the spacecraft. A detailed description of UARS is given in Ref. 3. Onboard disturbances were caused by UARS' five gimballed instruments and subsystems, attitude control reaction wheels, and propulsion subsystem, as well as the thermal elastic bending (thermal snap) of the solar array as the spacecraft passed through the Earth's terminator.[3–9] Many of these disturbances were triggered by the spacecraft's position in orbit, such as the thermal snap of the solar array or the HALOE events during orbital sunrise and sunset. Some disturbances were the result of UARS' relative position to other spacecraft, such as the high-gain antenna's line of sight to the Tracking and Data Relay Satellites (east and west) in geostationary orbits. These disturbances affected the precision pointing of the remote sensing instruments and coregistration of measurements.

To have produced accurate measurements, each instrument must have had its line-of-sight pointing jitter maintained within acceptable levels. Knowledge of the spacecraft orientation was provided by the attitude control system. The UARS attitude control system had several onboard sensors for attitude determination; however, only the rate gyros in the Inertial Reference Unit (IRU) could determine attitude to the precision needed for a jitter study. These gyros had a resolution of 0.05 arc-s (one telemetry count) and a sampling rate of 7.8125 Hz (Refs. 3 and 6).

Jitter Amplitude Variation with Solar Array Rotation

UARS' solar array positions are shown in Fig. 2 (Ref. 3). The angle was measured from the spacecraft's Y–Z plane. The orientation of the solar panels changed 360 deg each orbit. When the solar array vibrated, its vibration was imparted to the spacecraft and resulted in spacecraft vibration. Because of conservation of momentum, the vibration was scaled so that its maximum amplitude occurred when the tip inertia was the spacecraft roll inertia I_r, and its minimum amplitude occurred when the tip inertia was the spacecraft yaw inertia I_y. The I_r, I_p, and I_y for UARS are 13,400, 35,209, and 39,974 ft-lb s^2, respectively. When the solar array was rotating at the orbital angular velocity ω_0, the tip inertia varied as

$$I_{\text{tip}}(t) = \left(\frac{I_y + I_r}{2}\right) + \left(\frac{I_y - I_r}{2}\right)\sin(2\omega_0 t) \tag{1}$$

and the corresponding vibration amplitude $\theta(t)$ varied (assuming a disturbance with constant amplitude and transmission path) as

$$\theta(t) = \left(\frac{\theta_{\max} + \theta_{\min}}{2}\right) + \left(\frac{\theta_{\max} - \theta_{\min}}{2}\right)\cos(2\omega_0 t) \tag{2}$$

The vibration amplitude $\theta(t)$ was dependent on the tip inertia. By the time integral of conservation of momentum,

$$I_y \theta_{\min} = I_r \theta_{\max} \tag{3}$$

The variation of spacecraft median roll and yaw jitter (from day 233 past spacecraft launch) with solar array rotation is shown in Fig. 3. When the solar array was in the 90/270 deg position, the edgewise mode vibrated about an axis parallel to the spacecraft yaw axis, and the flatwise mode vibrated about the roll axis. When the solar array was in the 360/180 deg position, the edgewise mode vibrated about an axis parallel to the spacecraft roll axis, and the flatwise mode vibrated about the yaw axis. Therefore, the peaks for yaw and roll median jitter occurred at the 90/270 deg and 360/180 deg positions, respectively. Thus, results shown in Fig. 3 demonstrate that the solar array edgewise mode was the dominant mode of vibration. The nonharmonic amplitude variation of the solar array edgewise

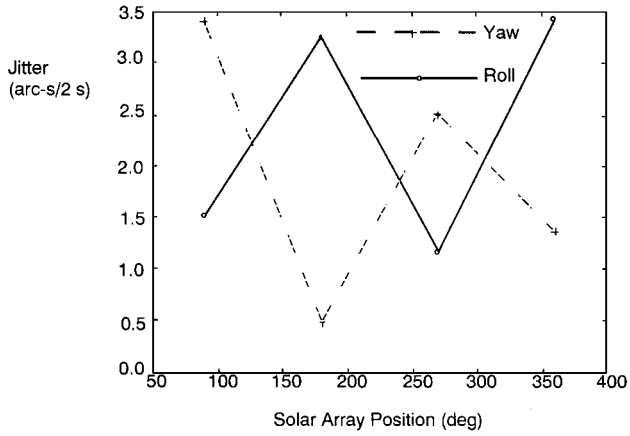

Fig. 3 Variation of median roll and yaw jitter with solar array position.

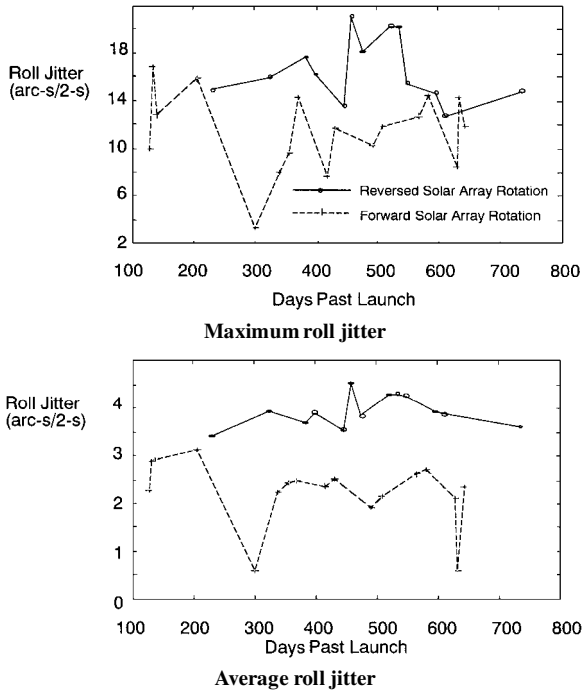

Fig. 4 Spacecraft roll jitter for day 128 through day 737 past launch.

mode indicates that the disturbance transmitted to the mode was not constant.

Figure 4 shows the maximum and average roll jitter for days 128 through 737 past the launch of UARS. The effect of the solar array rotation direction is apparent. The averages and maxima shown in Fig. 4 excluded jitter during the thermal bending of the solar array. Because of the precession of the orbit plane, the β angle swept out an angle of ± 80.45 deg (Ref. 2). The β angle is the complement of the angle between the orbit normal and the Earth-to-sun vector.[3,9] At large values of the β angle, solar array energy collection and sun impingement on the payloads became a problem. To alleviate the problem, the spacecraft was rotated 180 deg about its yaw axis approximately every 30–36 days. After each yaw maneuver, the direction of solar array rotation was changed. When the solar array was rotating in reversed direction, the jitter was higher than when the solar array was rotating in the forward direction, as shown in Fig. 4. The UARS jitter requirement was 4 arc-s/2 s. The significance of this finding (Fig. 4) is that the requirement was violated more during days when the solar array was rotating in the reverse direction. Hence, the accuracy of scientific measurements, which had to adhere to the 4 arc-s/2-s requirement, varied approximately every other month.

Because the orbit plane precessed between yaw maneuvers, the tracking instruments varied their tracking trajectories correspondingly. The change in tracking trajectories produced a corresponding change in the spacecraft response. Figure 5 shows the variation in

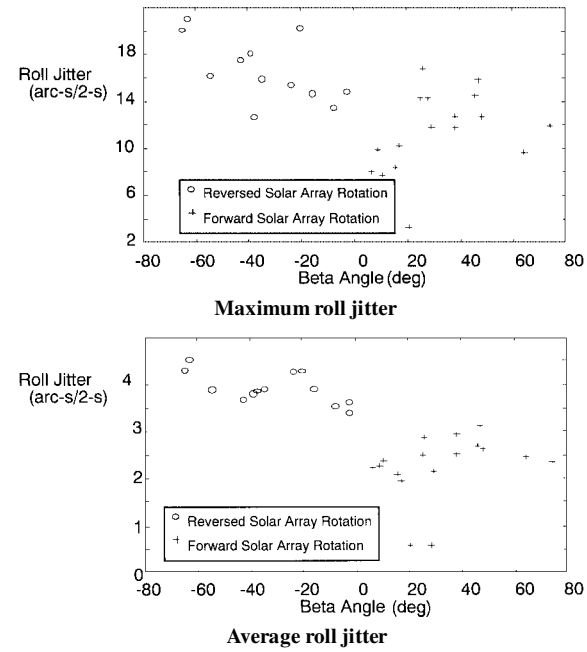

Fig. 5 Spacecraft roll jitter variation with β angle for day 128 through day 737 past launch.

spacecraft roll jitter with β angle for the same days used in Fig. 4. Jitter measurements during thermal bending of the solar array were also excluded from the results shown in Fig. 5. The dominant trend observed was that, as the magnitude of the β angle increased, the roll jitter increased. However, the values in the reversed direction were higher than those in the forward direction of solar array rotation. It can be inferred from Fig. 4 that, between yaw maneuvers, the jitter levels grew monotonically.

Appendage Modal Variation with Solar Array Rotation

One effect of variable spacecraft mass and inertia on appendage transverse vibration was the changing modal frequencies and mode shapes. Reference 3 has presented a detailed development and examination of the Euler beam equation with the appropriate boundary conditions, which showed short-term (orbital) periodic changes in modal characteristics when flexible appendages rotated and long-term effects due to mass expenditure (either fuel or cryogen expenditures or both). The characteristic equation for the Euler beam resulting from Ref. 3 is as follows:

$$\lambda_n^4[1-\cos(\lambda_n\ell)\cosh(\lambda_n\ell)] + \lambda_n\left(\frac{m_{\text{tip}}\omega_n^2}{EI}\right)[\sin(\lambda_n\ell)\cosh(\lambda_n\ell)-\cos(\lambda_n\ell)\sinh(\lambda_n\ell)] + \lambda_n^3\left(\frac{I_{\text{tip}}\omega_n^2}{EI}\right)[\cos(\lambda_n\ell)\sinh(\lambda_n\ell)+\sin(\lambda_n\ell)\cosh(\lambda_n\ell)] + I_{\text{tip}}m_{\text{tip}}\left(\frac{\omega_n^2}{EI}\right)^2[1+\cos(\lambda_n\ell)\cosh(\lambda_n\ell)] = 0 \quad (4)$$

Every combination of boundary conditions, i.e., tip mass and inertia, resulted in different frequencies and mode shapes. However, the frequencies and mode shapes varied from those of a free-free beam to those of a clamped-free beam as the mass and inertia both approached infinity. The characteristic equation, Eq. (4), results in the following combinations of frequencies and mode shapes: that of the free-free beam with no tip mass and no tip inertia, fixed-free for infinite tip mass and infinite tip inertia, sliding-free for infinite inertia and no tip mass, and pinned-free for infinite mass and no tip inertia. The natural frequency of the nth mode is given as

$$\omega_n = (\lambda_n\ell)^2\sqrt{EI/\rho\ell^4} \quad (5)$$

The results demonstrate that using free-free mode shapes for flexible appendages is valid only for spacecraft with small values of mass and inertia. The cantilever mode shapes are valid only for large values of inertia and mass. All values of mass and inertia between zero and infinity have modal properties that are dependent on Eq. (4). Equation (4) demonstrates that orbital variation in the tip inertia (as the solar array rotates) caused variations in modal frequencies and mode shapes. The variations were harmonic and exhibited a frequency of twice the orbital rate.

As shown in Fig. 6, a consequence of this analysis is that when the modal frequencies varied with orbit so did the potential for resonance due to instrument disturbances. The two resonance peaks shown in Fig. 6 are those for the end frequencies of a modal band. A modal band is the resulting range of frequencies that a mode of vibration can have as the result of a harmonic change in boundary condition, e.g., rotation of tip inertia. The resonance peak varied harmonically throughout an orbit (two cycles per orbit). As mass is expended, e.g., fuel for orbit adjust and cryogen sublimation, spacecraft mass and inertia will be reduced, and the modal band will be shifted to increasing frequency. Figure 7 shows the range of the UARS' solar array flatwise and edgewise frequencies measured from day 128 through day 737 for the 90-, 180-, 270-, and 360-deg positions. At each position, there was a spread of the frequencies. However, the lower and upper extremities of the spread were harmonic with respect to the 360 deg of rotation. This harmonic variation of the extremities is indicative of modal bands. The modal band is defined by the highest frequency observed (0.29 Hz at 180 deg) and the lowest frequency observed (0.21 Hz at 90 deg). Figure 7 also shows the output frequencies of the harmonic drives for the solar array (0.23 Hz), the high-gain antenna (HGA; 0.22 Hz), and the gimballed instrument mount (SSPP; 0.22 Hz). The harmonic drive output frequencies overlapped the modal band. The implication is that, during the orbit, each of the three harmonic drives was in transitory resonance with the solar array flatwise and edgewise modes of vibration. Furthermore, the combination of the three transitory resonances possibly contributed to the nonharmonic vibration amplitude variation of the solar array edgewise mode of vibration (Fig. 3).

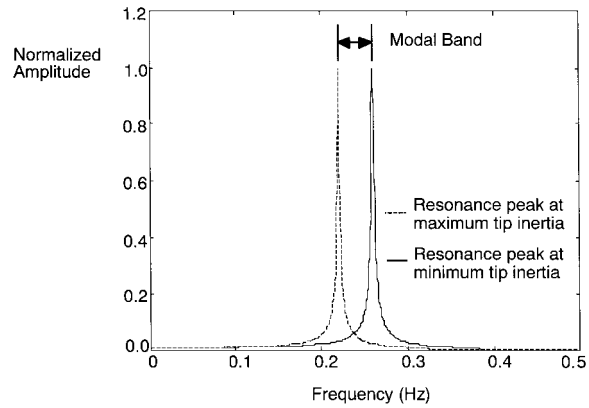

Fig. 6 Structural resonance peak displacement and modal band resulting from solar array rotation.

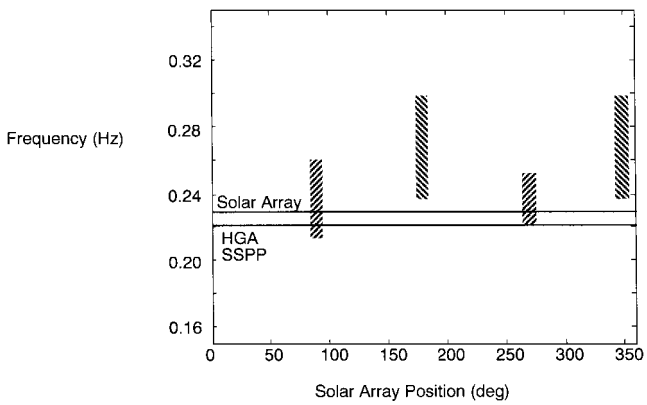

Fig. 7 Solar array modal frequency range measured from day 128 through day 737 past launch for 90-, 180-, 270-, and 360-deg positions.

Another implication of this result is that, when one considers structural models in control design, modal bands must be considered instead of discrete frequencies. Controller design must be robust enough to accommodate entire bands. Furthermore, controllers conceived via optimization strategies are usually designed about some nominal configuration. Thus, variations in modal properties will result in suboptimal control performance for all other configurations.

Disturbance Transmission Variation with Solar Array Rotation

Many onboard spacecraft disturbances had fixed points of application and fixed directions of force or torque. Their transmission through the spacecraft was constant. However, the resulting disturbance response due to rotating flexible appendages varied with the appendage orientation to the disturbance source.[3] This was true for all disturbances except for the solar array drive mechanism. The mode shapes changed (owing to varying tip inertia from rotation) their orientation with respect to the disturbances. The overall dynamical system can be generalized as

$$\dot{\boldsymbol{X}} = \boldsymbol{AX} + \boldsymbol{BU}, \qquad \boldsymbol{Y} = \boldsymbol{CX} \tag{6}$$

with $\boldsymbol{U}$ fixed and

$$\boldsymbol{B}^T = [\boldsymbol{0} \quad \Gamma(\boldsymbol{X}, t)] \tag{7}$$

The mode shapes $\Gamma(\boldsymbol{X}, t)$ varied harmonically with a frequency of twice the solar array rotation frequency (orbital frequency). With fixed disturbances imparted to the rotating solar arrays, the resulting jitter response had amplitude variations that were also harmonic and in synchronization with twice the solar array rotation rate. Because the spacecraft's latitude varied with solar array rotation, the resulting jitter response was latitude specific.[6] This result was significant because atmosphere-observing satellites may attribute measurements that appeared as latitude specific to be due to atmospheric phenomena when they were actually due to the latitude-specific vibration pattern of the platform from which measurements were taken. Furthermore, because this result was due to variation of mode shape orientation with respect to fixed disturbances, this effect was independent of the tip inertia variation due to rotation of the solar array.

Thermal Elastic Bending Variation with Orbit and Orbital Precession

This section presents analyses of environmental disturbance effects that resulted from the temperature gradient created when a spacecraft entered or exited the Earth's terminator. As a spacecraft's appendage entered sunlight, the side facing the sun heated at a faster rate than the side not facing the sun.[8,9] The thermal gradient caused the appendage to bend away from the sun. As the spacecraft entered the Earth's shadow, the side facing the sun cooled more rapidly than the other side. The solar array temperature gradient was inversely dependent on the β angle. Thermal bending is illustrated in Fig. 8. The bending resulted in an attitude perturbation.

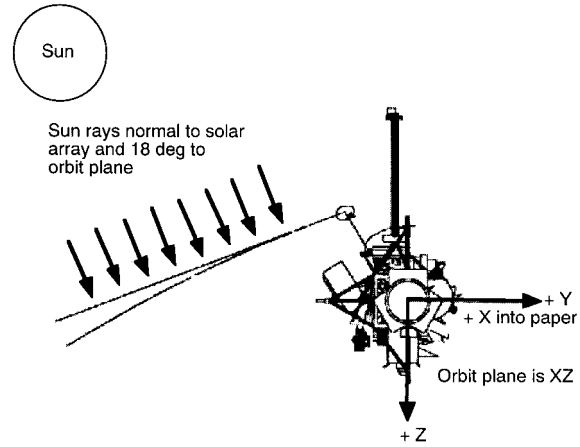

Fig. 8 Bending of UARS solar array at orbital terminator crossing.

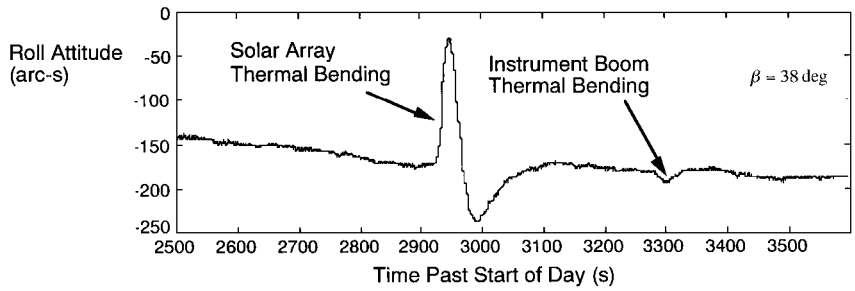

a) Thermal bending on 139th day after launch

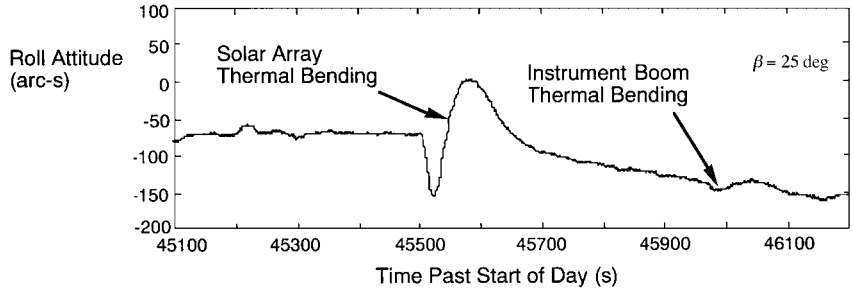

b) Thermal bending on 370th day after launch

Fig. 9 UARS attitude response to thermal elastic bending of the solar array and instrument boom.

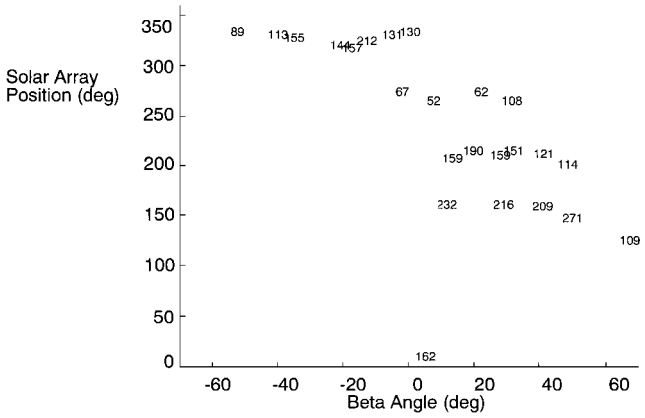

Fig. 10 Variation of sunrise thermal snap trough-to-peak roll attitude displacement with solar array position and β angle.

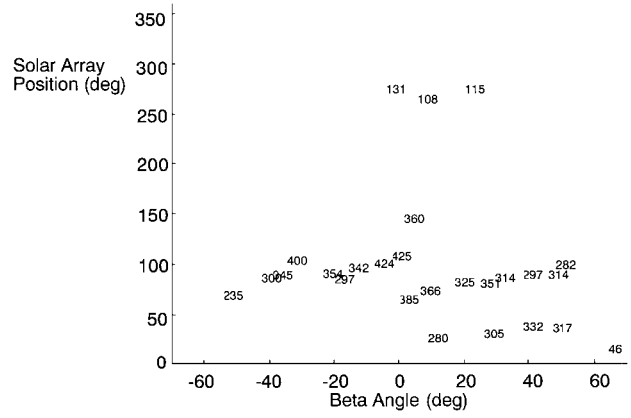

Fig. 11 Variation of sunset thermal snap trough-to-peak roll attitude displacement with solar array position and β angle.

Perturbations were more pronounced about the spacecraft roll axis (axis of least inertia). The larger perturbations were caused by the solar energy incident upon the large surface area of the array panel and the panel's large mass moment of inertia about the spacecraft roll axis. The spacecraft attitude control system responded to the change in attitude with a correcting torque that restored the spacecraft's nominal attitude.

The thermal bending of the solar array was the most pronounced disturbance event recorded with the attitude control system rate gyros. Figure 9 shows the roll attitude during two orbital sunrises for two orbits with different β angles. These angles are indicated in Figs. 9a and 9b. The peaks in Fig. 9, caused by solar array thermal bending, are approximately 125 arc-s and 75 arc-s for β angles of 25 and 38 deg, respectively. In addition to thermal bending, the solar array shadow temporarily shielded the instrument boom containing the Zenith Energetic Particle System instrument from the sun. This resulted in the thermal elastic bending of that boom being delayed by 300–400 s. The delay varied inversely with the β angle. The instrument boom bending effects were less pronounced because of the smaller solar incident surface area and smaller mass inertia. Furthermore, the bending stiffness for the instrument boom was an order of magnitude higher than that of the solar array. Much attention has been focused on the solar array thermal bending and its effect on the scientific measurements. However, the instrument boom produced a roll attitude displacement of 12 arc-s. This displacement may also have had some marginal effect on the measurements.

Data from orbits were examined at approximately 15-day intervals from days 128 through 737 past launch. The trough-to-peak roll attitude displacement and displacement duration were measured for each orbital sunset and sunrise thermal bending event. The displacements were then correlated with the β angle and solar array orientation during the displacement. Figures 10 and 11 show the trough-to-peak roll attitude displacement resulting from thermal bending of the solar array during orbital sunrise and sunset, respectively. The displacements are annotated (rounded to nearest arc-s) for the respective β angle and solar array position. The magnitude of roll attitude perturbation was dependent on the β angle and solar array orientation with respect to the drive shaft.

During orbital sunrise (Fig. 10) the displacement was larger for β angles near 17 deg and solar array orientations of 160 deg. The sunrise attitude displacements were as high as 271 arc-s. During orbital sunset (Fig. 11), the displacement was larger for β angles near 0 deg and solar array orientations near 90 deg. The sunset attitude displacement was as high as 425 arc-s. The perturbation events were usually 180 s in duration. Duration was dependent on the β angle and the solar array orientation with respect to its drive shaft. The solar array completed approximately $\frac{1}{3}$ revolution between sunset and sunrise. When the solar array was oriented at 90 deg (or 270-deg position) for maximum electrical power production, it also experienced the maximum attitude perturbation for sunset (sunrise).

The effect of spacecraft mass loss on thermal bending was also examined. The UARS' cryogen was completely outgassed on

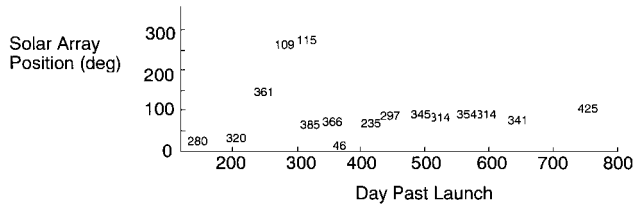

a) Roll attitude displacement during sunset thermal snap (arc-s)

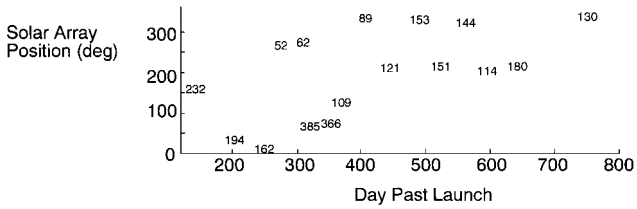

b) Roll attitude displacement during sunrise thermal snap (arc-s)

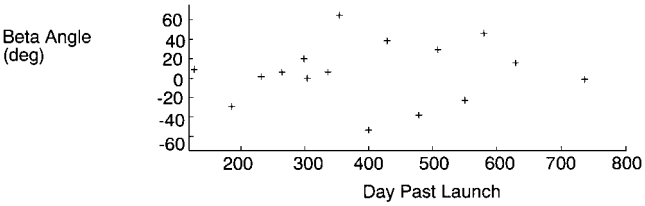

c) β angle during thermal snaps

Fig. 12 Sunset and sunrise thermal snap peak-to-peak displacement variations with solar array position and orbital solar incidence angle.

May 5, 1993 (day 603 past launch). The UARS' launch weight was 14,820 lb. Approximately 7% of UARS' mass was outgassed. The mass loss should have resulted in the perturbation amplitude changing approximately 7%. Perturbations varied 180% owing to variations in β angles. Perturbations varied 323% because of variations in solar array orientation angles. Figures 12a and 12b show the roll attitude displacements from days 128 through 737 for sunset and sunrise thermal snaps, respectively. The displacements were referenced to the solar array position (ordinate) and day past launch (abscissa). The displacements were annotated in a way similar to the approach used in Figs. 10 and 11. The β angles for the displacements given in Figs. 12a and 12b are given in Fig. 12c. The effect of changing solar array position or β angle dominated the influence of thermal bending. Measurement of mass loss effects on thermal bending was not discernible because of those effects.

The UARS must meet a long-term stability requirement of bounding roll attitude displacement to 108 arc-s during any 60-s interval. Many of the perturbations examined violated this requirement. The stability requirements were necessary for interpretation of scientific data. Analysis has shown that the thermal bending of the solar array results in trough-to-peak roll attitude displacements of 425 arc-s during a 47-s interval. The perturbations have also been observed on LANDSAT 4 and 5. Symmetric dual-solar-array satellites experienced such perturbations, but they are more pronounced for asymmetric single arrays. When unobstructed viewing from space is required, such as on UARS or the Earth Observing System A.M. satellite, it is necessary to use single-array spacecraft. Because the perturbations violated the long-term stability requirements and can be expected for single-array spacecraft, it is critical that spacecraft designers have valid dynamic models to predict the response to thermal bending.

Concluding Remarks

Analysis using the Upper Atmosphere Research Satellite (UARS) flight data from the first 737 days past launch has provided better understanding of UARS in-flight dynamics. Although UARS had many disturbance sources, orbital and configuration changes greatly influenced the dynamic response. Flight data have shown that modal frequencies and jitter amplitudes varied with a frequency of twice the solar array rotation rate. The variation of the solar array modal frequencies (near 0.25 Hz) produced a modal band. Within the band, the resonance frequency varied harmonically. Three UARS disturbances had frequencies that overlapped the modal band and thus produced a transitory resonance. Another consequence of modal variations due to configuration change was that disturbance transmission was also dependent on the modal properties of the system. Hence, as the modal properties changed, the disturbance transmission path changed.

The precession of the orbit caused the β angle to increase. Solar and stellar tracking instruments adjusted their tracking trajectories to accommodate the precession. The increased tracking activity produced higher disturbance levels, which resulted in higher jitter amplitudes as the β angle increased. Between yaw maneuvers, the jitter increased monotonically. The direction of solar array rotation also had a pronounced effect on the subsequent jitter levels. The reversed solar array rotation resulted in higher jitter amplitudes than forward rotation.

Analysis of the thermal elastic bending of the solar array has shown the effect of β angle and the solar array orientation on the spacecraft dynamic response. Trough-to-peak amplitude variation was as high as 425 arc-s. During sunset, the bending was higher for β angles near 0 deg and solar array orientations near 90 deg. The roll attitude perturbations resulting from the solar array bending varied 180% owing to β angle variations and 323% as the result of solar array orientation variations. The effect of the 7% mass loss on the thermal bending perturbations was not discernible because of the effects of array orientation variations and β angle variations.

The results of studying the in-flight dynamics of UARS have shown the significance of spacecraft inertia variations on the modal characteristics of flexible appendages and on spacecraft jitter. Furthermore, results of these analyses can be extended to spacecraft with similar dynamic characteristics such as the Mir and the International Space Station.

Acknowledgments

The author thanks William L. Grantham, Jerry Newsom, and Veloria J. Martinson at NASA Langley Research Center; Ansel J. Butterfield of Bionetics Corporation; and Joseph Laufer for their support in this research.

References

[1] "Upper Atmosphere Research Satellite Project Data Book," Astro-Space Div., General Electric Co., Valley Forge, PA, April 1987.

[2] "Upper Atmosphere Research Satellite Command and Telemetry Handbook," Astro-Space Div., General Electric Co., SDS-4219, Valley Forge, PA, Jan. 1991.

[3] Woodard, S. E., "The Upper Atmosphere Research Satellite In-Flight Dynamics," NASA TM 11035, April 1997.

[4] Molnar, J., and Garnek, M., "UARS In-Flight Jitter Study for EOS," NASA CR 191419, Jan. 1993.

[5] Butterfield, A. J., and Woodard, S. E., "Measured Spacecraft Instrument and Structural Interactions," *Journal of Spacecraft and Rockets*, Vol. 33, No. 4, 1996, pp. 556–562.

[6] Woodard, S. E., Lay, R., Jarnot, R., and Gell, D., "Experimental Investigation of Spacecraft In-Flight Disturbances and Dynamic Response," *Journal of Spacecraft and Rockets*, Vol. 34, No. 2, 1997, pp. 199–204.

[7] Mills, R., and Garnek, M., "UARS Dynamic Disturbance Torque Analysis," Astro-Space Div., General Electric Co., PIR U-1K21-UARS-279, PIR U-1R44-UARS-1351, Valley Forge, PA, Nov. 1985.

[8] Zimbelman, D. F., "Thermal Elastic Shock and Its Effect on Topex Spacecraft Attitude Control," 14th Annual American Astronautical Society Guidance and Control Conf. (Keystone, CO), AAS Paper 91-056, Feb. 1991.

[9] Lambertson, M., Underwood, S., Woodruff, C., and Garber, A., "Upper Atmosphere Research Satellite Attitude Disturbances During Shadow Entry and Exit," American Astronautical Society, AAS Paper 93-319, Aug. 1993.

J. D. Gamble
Associate Editor